Article

Succinimide Formation from an NGR-Containing Cyclic Peptide: Computational Evidence for Catalytic Roles of Phosphate Buffer and the Arginine Side Chain

Ryota Kirikoshi, Noriyoshi Manabe and Ohgi Takahashi *

Faculty of Pharmaceutical Sciences, Tohoku Medical and Pharmaceutical University, 4-4-1 Komatsushima, Aoba-ku, Sendai 981-8558, Japan; kirikoshi@tokoku-mpu.ac.jp (R.K.); manabe@tohoku-mpu.ac.jp (N.M.)
* Correspondence: ohgi@tohoku-mpu.ac.jp; Tel.: +81-022-727-0208

Abstract: The Asn-Gly-Arg (NGR) motif and its deamidation product *iso*Asp-Gly-Arg (*iso*DGR) have recently attracted considerable attention as tumor-targeting ligands. Because an NGR-containing peptide and the corresponding *iso*DGR-containing peptide target different receptors, the spontaneous NGR deamidation can be used in dual targeting strategies. It is well known that the Asn deamidation proceeds via a succinimide derivative. In the present study, we computationally investigated the mechanism of succinimide formation from a cyclic peptide, c[CH$_2$CO-NGRC]-NH$_2$, which has recently been shown to undergo rapid deamidation in a phosphate buffer. An H$_2$PO$_4^-$ ion was explicitly included in the calculations. We employed the density functional theory using the B3LYP functional. While geometry optimizations were performed in the gas phase, hydration Gibbs energies were calculated by the SM8 (solvation model 8) continuum model. We have found a pathway leading to the five-membered ring tetrahedral intermediate in which both the H$_2$PO$_4^-$ ion and the Arg side chain act as catalyst. This intermediate, once protonated at the NH$_2$ group on the five-membered ring, was shown to easily undergo NH$_3$ elimination leading to the succinimide formation. This study is the first to propose a possible catalytic role for the Arg side chain in the NGR deamidation.

Keywords: Asn-Gly-Arg (NGR) motif; *iso*Asp-Gly-Arg (*iso*DGR) motif; tumor-targeting ligands; deamidation; nonenzymatic reaction; succinimide intermediate; phosphate buffer catalysis; intramolecular catalysis; computational chemistry; density functional theory

1. Introduction

Deamidation of asparagine (Asn, N) residues is one of the most common reactions which occur nonenzymatically in peptide chains. A succinimide species is known to be the intermediate of Asn deamidation (Scheme 1) [1–11]. This intermediate having a five-membered ring is formed by the nucleophilic attack of the main-chain nitrogen atom of the C-terminal adjacent residue on the Asn side-chain amide carbon with release of an ammonia molecule. This is an intramolecular nucleophilic substitution reaction and is generally considered to occur in two steps (cyclization-deammoniation, Scheme 2) [12,13]. In the first step, the nucleophilic attack gives rise to a five-membered ring tetrahedral intermediate. In the second step, an NH$_3$ molecule is released from this intermediate to give the succinimide species. Hydrolysis of the succinimide intermediate can occur at either of its two carbonyl groups, leading to the formation of aspartic acid (Asp, D) and isoaspartic acid (β-aspartic acid) (*iso*Asp, *iso*D) residues in a typical ratio of 1:3 [1–7]. Small amounts of D-Asp and D-*iso*Asp residues may also be formed via racemization of the succinimide intermediate [1,7,14,15]. While the Asn deamidation in proteins and peptides is often regarded as a degradation reaction, a "molecular clock" hypothesis was

proposed which claims that the Asn deamidation regulates the timing of biological processes such as protein turnover [8–10]. It is well known that the rates of Asn deamidation are greatly dependent on the neighboring amino acid residue on the C-terminal side and are generally by far the fastest when this residue is glycine (Gly, G), the smallest amino acid residue [1,3,5–9].
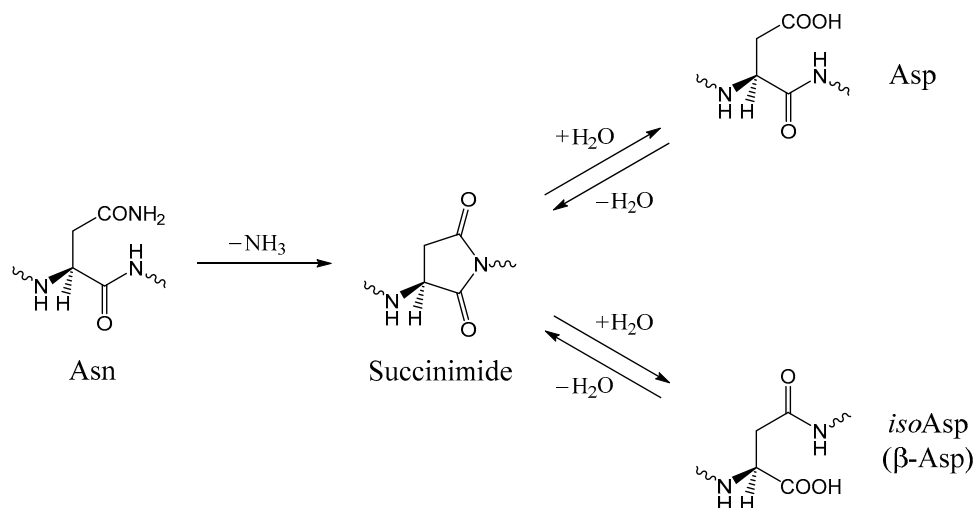
Scheme 1. Succinimide-mediated deamidation of an Asn residue giving *iso*Asp (β-Asp) and Asp residues.
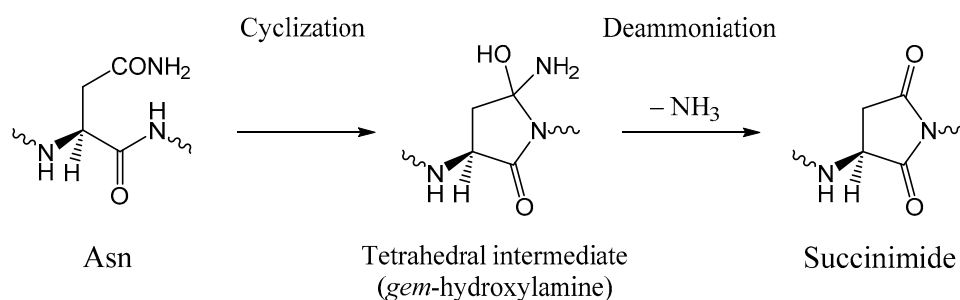

Scheme 2. Two-step (cyclization-deammoniation) mechanism for the succinimide formation from an Asn residue.

Recently, peptides containing the asparagine-glycine-arginine (Asn-Gly-Arg, NGR) motif [16–75] and their deamidation products containing the *iso*DGR motif [38,41,46,48,56,59,74,76–85] have attracted considerable attention as tumor-targeting ligands. The tumor-targeting property of the NGR motif was first reported by Ruoslahti and co-workers in 1998 [16], and then it was revealed that peptides containing the NGR motif bind to an aminopeptidase N (APN or CD13) isoform which is uniquely expressed on the endothelium of tumor vasculature [18,22]. It was later that the *iso*DGR-containing peptides (but not DGR-containing peptides), especially cyclic ones, bind to $\alpha_v\beta_3$ integrin which is also overexpressed in tumor cells including the vascular endothelium [38,48,76,77]. NGR-containing peptides thus may be used for dual targeting strategies in specifically targeted delivery of various drugs, imaging agents, etc., to tumors [38,41,59,71,74,82], and clarifying the detailed mechanism of the NGR-to-*iso*DGR transition will be helpful in designing dual targeting ligands with desired properties.

Very recently, Enyedi and co-workers have shown that several NGR-containing cyclic peptides with a 15- to 18-membered ring undergo very rapid deamidation [71]. Among those, c[CH$_2$CO-NGRC]-NH$_2$ (Figure 1) having a cysteine (Cys, C) thioether linkage in a 15-membered ring deamidated most rapidly in phosphate-buffered saline (PBS, pH 7.4) at room temperature. More specifically, 68% and 17% of the peptide were converted to the corresponding *iso*DGR and

DGR peptides, respectively, after 48 h incubation. It should be noted that the peptide was stable in distilled or slightly acidic water at room temperature for 48 h. Therefore, the phosphate buffer is considered to catalyze the deamidation. Hereafter, we denote the 15-membered cyclic peptide, c[CH$_2$CO-NGRC]-NH$_2$, as CP15.
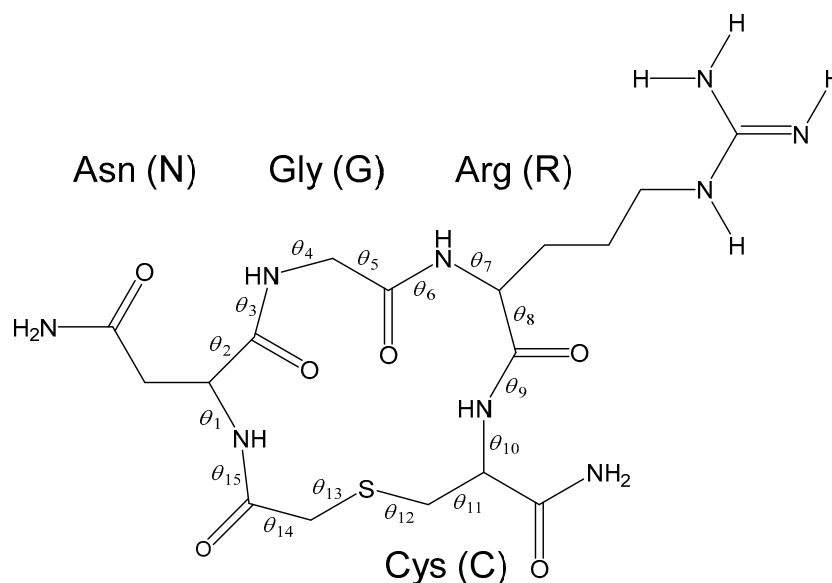
Figure 1. A 15-membered cyclic peptide, c[CH$_2$CO-NGRC]-NH$_2$, containing the NGR (Asn-Gly-Arg) motif. This peptide is called CP15 in this paper. The guanidino group of the Arg side chain is depicted as a deprotonated form (see text for details). The definition of the heavy-atom dihedral angles θ_1–θ_{15} for the 15-membered ring are also shown.

In a recent paper, we have computationally shown that glycolic acid (in its protonated form) can catalyze Asn deamidation at a low pH [12]. In the mechanism we have revealed, a glycolic acid molecule acts as both proton donor and acceptor in double proton transfers. A similar mechanism may also operate in the phosphate-catalyzed deamidation in the NGR motif.

In the present study, we have computationally revealed a phosphate-catalyzed mechanism for the succinimide formation from CP15. The Arg residue also plays a catalytic role in that it contributes to fixing a catalytic H$_2$PO$_4^-$ ion in the right position for the first step (i.e., the formation of the tetrahedral intermediate). It is also shown that the tetrahedral intermediate, once protonated at the NH$_2$ group on the five-membered ring, easily releases an NH$_3$ molecule to form the succinimide species.

2. Results and Discussion

Figure 2 shows the energy profile in water obtained from the present calculations, and Figures 3–9 show optimized geometries. The geometry optimizations were performed in the gas phase by the density functional theory (DFT) with the B3LYP functional and the 6-31G(d) basis set, and the electronic energies were recalculated by using the 6-31+G(d,p) basis set at the optimized geometries. Furthermore, hydration Gibbs energies were calculated at the gas-phase optimized geometries by the SM8 (solvation model 8) continuum model [86,87] using the 6-31G(d) basis set. Relative energies were also corrected for the zero-point energy (ZPE). The Cartesian coordinates, total energies, ZPEs, and SM8 hydration Gibbs energies of the optimized geometries are provided in Tables S1–S7.
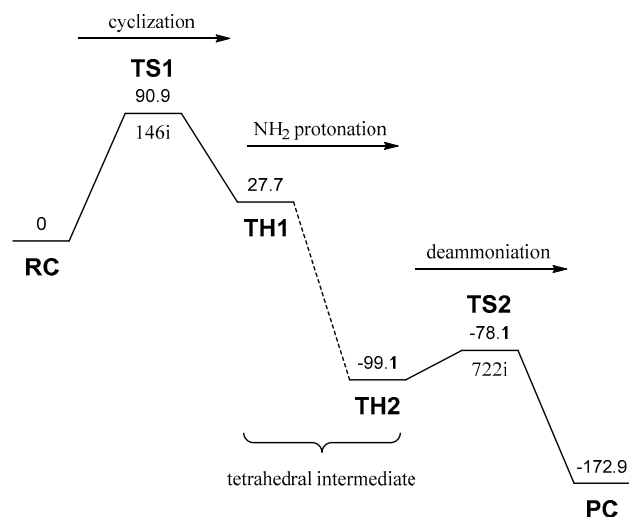
Figure 2. Energy profile in water. RC: reactant complex; TS: transition state; TH: tetrahedral intermediate; PC: product complex. The relative energies with respect to RC are shown in kJ·mol^{-1}. The imaginary frequencies for the two transition states are also shown.

Figure 3 shows the optimized geometry of the reactant complex (RC) formed between CP15 (in the deprotonated form as shown in Figure 1) and an $H_2PO_4^-$ ion. This geometry was obtained by an intrinsic reaction coordinate (IRC) calculation (followed by a full geometry optimization) from the transition state TS1 (transition state of the first step) described below; the geometry of TS1 was obtained after some trial and error. At pH 7.4, however, Arg side chains are in the protonated form, and HPO_4^{2-} is the dominating phosphate species. We therefore attempted to find a complex between CP15 in the protonated form and an HPO_4^{2-} ion near the RC geometry. However, in all attempts, a spontaneous proton transfer occurred from the protonated guanidino group to the HPO_4^{2-} ion during geometry optimization. Since a reasonable activation barrier was obtained from RC (see below), we deduce that complex formation between CP15 and an HPO_4^{2-} ion accompanies a simultaneous proton transfer from the former to the latter.
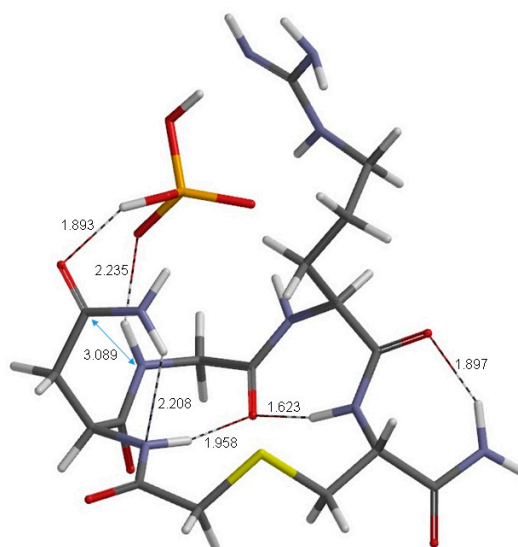
Figure 3. The geometry of the reactant complex (RC) formed between the cyclic peptide CP15 (in a deprotonated form as shown in Figure 1) and an $H_2PO_4^-$ ion. Selected interatomic distances are shown in Å. Grey: carbon; white: hydrogen; blue: nitrogen; red: oxygen; orange: phosphorus; yellow: sulfur.

In RC (reactant complex), a nine-point interaction is observed between CP15 and the $H_2PO_4^-$ ion comprising six hydrogen bonds and three CH–O interactions. These nine interactions are shown in Figure 4 as a–i, and the corresponding interatomic distances are shown in Table 1 (note that one of the two Arg β-protons is involved in a bifurcated CH–O interaction, the d and e interactions in Figure 4). It may be said that an HPO_4^{2-} ion is efficiently recognized by the NGR motif of CP15 accompanied by a proton transfer. Interactions a and b are hydrogen bonding between the deprotonated guanidino group and the $H_2PO_4^-$ ion. The main-chain NH group of Arg also forms a hydrogen bond to $H_2PO_4^-$ (the interaction c). It is important that the neighboring amino acid residue of Asn on the C-terminal side is Gly. Otherwise, a pocket which can accommodate an $H_2PO_4^-$ ion is not created because of the side chain. Indeed, the Gly α proton corresponding to the side chain of L-amino acid residues is involved in a CH–O interaction (the interaction i). Interactions h (2.235 Å) and g (1.893 Å) are important for the reaction because these are involved in the proton transfers which occur in the first step (see below). Interaction f involves the NH_2 group of the Asn side chain. As a result, the Asn side chain is placed in the right position to undergo the cyclization (C–N bond formation); the distance between the carbon and nitrogen atoms to form a bond is 3.089 Å in RC.
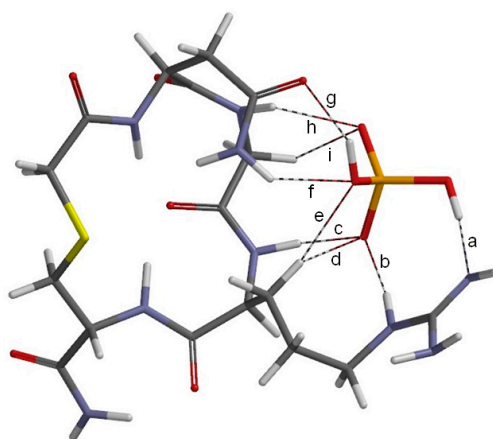
Figure 4. The nine-point interaction (interactions a–i) in RC (the reactant complex shown in Figure 3). The corresponding interatomic distances are shown in Table 1. Grey: carbon; white: hydrogen; blue: nitrogen; red: oxygen; orange: phosphorus; yellow: sulfur.

Table 1. Interatomic distances (Å) in RC (Figure 3), TS1 (transition state of the first step) (Figure 5), and TH1 (tetrahedral intermediate directly connected to TS1) (Figure 6) corresponding to the interactions a–i shown in Figure 4.

| Geometry	a	b	c	d	e	f	g	h	i
RC	1.824	1.789	1.713	2.361	2.421	2.196	1.893	2.235	2.306
TS1	1.745	1.828	1.805	2.482	2.584	2.135	1.070	0.978	2.531
TH1	1.747	1.840	1.750	2.509	2.738	2.104	1.001	0.977	2.355

Furthermore, we can see two hydrogen bonds involving the Gly C=O group inside the 15-memberd ring of RC (Figure 3), one to the Asn NH group (1.958 Å) and the other to the Cys NH group (1.623 Å); the latter is very short and is thought to have a large contribution to stabilizing the macrocycle conformation in RC. In Table 2, the heavy-atom dihedral angles θ_1–θ_{15} defined for the 15-membered ring, as in Figure 1, are shown.

The transition state TS1 shown in Figure 5 connects RC and TH1 (the tetrahedral intermediate directly connected to TS1, Figure 6). The activation barrier of the first step (cyclization to form the tetrahedral intermediate TH1) was calculated to be 90.9 kJ·mol^{-1} after the ZPE and hydration Gibbs

energy corrections. This value falls within the range of typical activation energies of Asn deamidation (80–100 kJ·mol^{-1}) [1,4,5,11]. The relative energy of TH1 with respect to RC is 27.7 kJ·mol^{-1}.

Table 2. The heavy-atom dihedral angles θ_1–θ_{15} (°) defined for the 15-membered ring as in Figure 1.

| Geometry	θ_1	θ_2	θ_3	θ_4	θ_5	θ_6	θ_7	θ_8	θ_9	θ_{10}	θ_{11}	θ_{12}	θ_{13}	θ_{14}	θ_{15}
RC	−146	−91	139	−78	−121	165	40	−33	−157	155	−63	159	−131	44	167
TS1	−165	−89	145	−91	−120	168	20	−18	−165	160	−64	158	−132	60	174
TH1	−172	−91	149	−85	−133	169	15	−14	−165	159	−63	165	−127	53	−179
TH2	−117	−115	166	−59	139	180	69	6	177	151	−82	175	−67	−35	162
TS2	−116	−112	169	−60	138	−180	68	7	177	151	−83	177	−68	−35	160
PC	−90	−108	170	−49	132	179	70	1	−179	152	−70	171	−57	−76	159
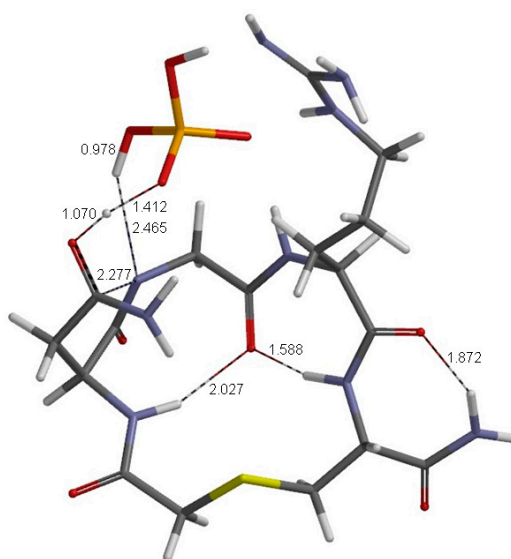
Figure 5. The geometry of TS1 (transition state of the first step) connecting RC (Figure 3) and TH1 (tetrahedral intermediate directly connected to TS1) (Figure 6). Selected interatomic distances are shown in Å. Grey: carbon; white: hydrogen; blue: nitrogen; red: oxygen; orange: phosphorus; yellow: sulfur.
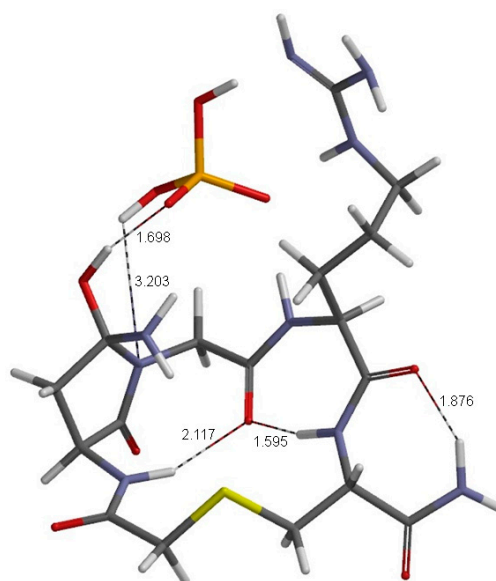
Figure 6. The geometry of TH1, the tetrahedral intermediate directly connected to TS1 (Figure 5). Selected interatomic distances are shown in Å. Grey: carbon; white: hydrogen; blue: nitrogen; red: oxygen; orange: phosphorus; yellow: sulfur.

At TS1, the NH proton of Gly has already been abstracted by the O atom in $H_2PO_4^-$ which had originally formed a hydrogen bond (the interaction h, 2.235 Å) to the NH proton in RC (the NH and OH distances in TS1 are 2.465 and 0.978 Å, respectively). Thus, the nucleophilicity of the Gly nitrogen is enhanced in the initial stage of the first step (note that amide nitrogens generally have low nucleophilicity [88]). The distance of the forming N–C bond in TS1 is 2.277 Å. On the other hand, another proton transfer is occurring from the $H_2PO_4^-$ ion to the Asn side-chain oxygen; this proton transfer is not completed at TS1 as may be seen from the relevant interatomic distances shown in Figure 5 (1.412 and 1.070 Å). All of these changes take place in a single step, leading to the formation of a five-membered ring tetrahedral intermediate TH1 (Figure 6) bearing an NH_2 and an OH group on the same carbon atom (a *gem*-hydroxylamine species). It should be noted that the two hydrogen bonds inside the 15-membered ring were maintained through the first step. In particular, the hydrogen bond involving the Cys NH group remained very short (1.588 and 1.595 Å in TS1 and TH1, respectively). Among the dihedral angles θ_1–θ_{15}, θ_1 and θ_7 show the largest changes (by about 26° and 25°, respectively) in the first step (Table 2); on the other hand, θ_2 and θ_{11} remained almost unchanged. The interactions a–f and i (Figure 4) were also preserved in the first step as may be seen from Table 1. Note that the proton transfers have occurred along the hydrogen bonds corresponding to the interactions g and h.

The NH_2 group on the five-membered ring of TH1 is expected to be easily protonated at neutral or physiological pH (see our recent paper [13]). Therefore, the second step (NH_3 release) was calculated for the NH_2-protonated form of the tetrahedral intermediate (TH2). Figure 7 shows the optimized geometry for TH2. The protonation induced a relatively large geometrical change and a considerable energy lowering. As to the 15-membered ring conformation, θ_5 and θ_{14} changed by about 88°, and θ_1, θ_7, and θ_{13} changed by more than 50°. See Figure 7 for the hydrogen bonding and CH–O interaction scheme in TH2. The two hydrogen bonds inside the 15-membered ring of TH1 have disappeared; instead, a new transannular hydrogen bond (2.186 Å) has been formed between the C=O group of the five-membered ring and the Cys NH group. The protonated NH_2 group is stabilized by two hydrogen bonds (1.456 and 1.840 Å).
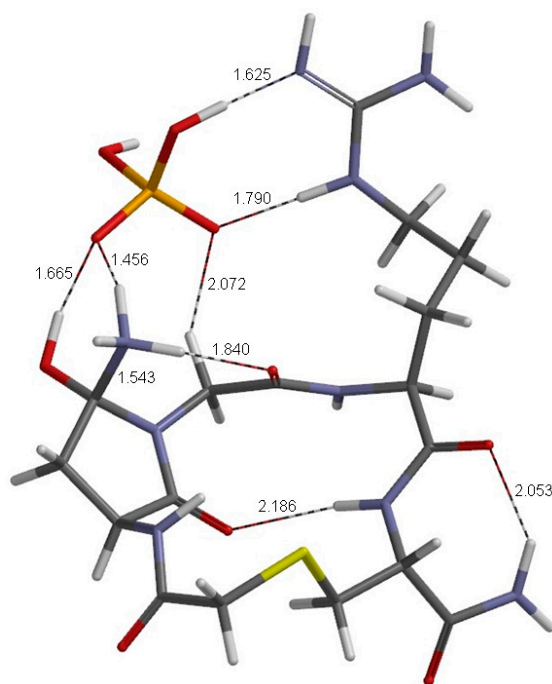

Figure 7. The geometry of TH2, the protonated tetrahedral intermediate directly connected to TS2 (Figure 8). Selected interatomic distances are shown in Å. Grey: carbon; white: hydrogen; blue: nitrogen; red: oxygen; orange: phosphorus; yellow: sulfur.

It should be noted that the energy of TH2 can not be directly compared to that of TH1 because of a different stoichiometry. In order to compare the energies of TH1 and TH2, we have added the recommended value of -265.9 kcal·mol^{-1} (1 cal = 4.184 J) for the hydration Gibbs energy of proton [89] to the energy of TH1 (note that the electronic energy of a bare proton is zero). This strategy is the same as the one we have employed in a recent paper [13]. The energy diagram shown in Figure 2 was obtained by adding this value to the energies of RC, TS1, and TH1. The protonation of TH1 at the NH$_2$ nitrogen resulted in stabilization as large as 126.8 kJ·mol^{-1}. This large value can be interpreted as follows. The experimental Gibbs energies of protonation for primary alkylamines (RNH$_2$) are about -60 kJ·mol^{-1} [90]. In the case of TH1/TH2, the protonated amino group is stabilized by two hydrogen bonds, one to the Gly oxygen (1.840 Å) and the other to the H$_2$PO$_4^-$ ion (1.456 Å); the latter is very short and, therefore, is thought to have a large stabilizing effect. Also, the neighboring OH group may have an additional stabilization effect on TH2.

From TH2, the departure of an NH$_3$ molecule (C–N bond cleavage) occurs via TS2 (the transition state of the second step) shown in Figure 8. At TS2, the distance of the cleaving C–N bond is 1.668 Å (the corresponding distance in TH2 was 1.543 Å). A double proton transfer also occurs in this second step from the OH group on the five-membered ring to the deprotonated guanidino group mediated by the H$_2$PO$_4^-$ ion, leading to the succinimide product with the protonated guanidino group. This double proton transfer is asynchronous as may be seen from the relevant interatomic distances shown in Figure 8. Whereas the proton transfer from the OH group to H$_2$PO$_4^-$ occurs in concert with the C–N bond cleavage, the transfer from H$_2$PO$_4^-$ to the guanidino group occurs in the latest stage of the second step. The local activation barrier for the second step is only about 21 kJ·mol^{-1}.
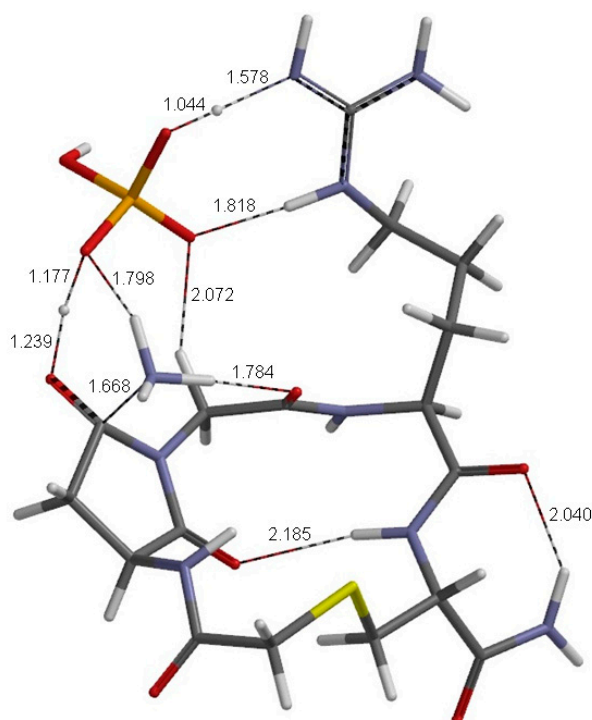

Figure 8. The geometry of TS2, the transition state of the second step (deammoniation) connecting TH2 (Figure 7) and PC (Figure 9). Selected interatomic distances are shown in Å. Grey: carbon; white: hydrogen; blue: nitrogen; red: oxygen; orange: phosphorus; yellow: sulfur.

Figure 9 shows the resultant product complex (PC), which comprises the succinimide product (in which the guanidino group of Arg is protonated), an H$_2$PO$_4^-$ ion, and an NH$_3$ molecule. In PC, the NH$_3$ molecule forms three hydrogen bonds, two to the product succinimide molecule and one to

the $H_2PO_4^-$ ion. The $H_2PO_4^-$ ion forms a total of five hydrogen bonds. The transannular hydrogen bond in the 15-membered ring was preserved through the second step. The relative energy of PC with respect to TH2 is -73.8 kJ·mol^{-1}.
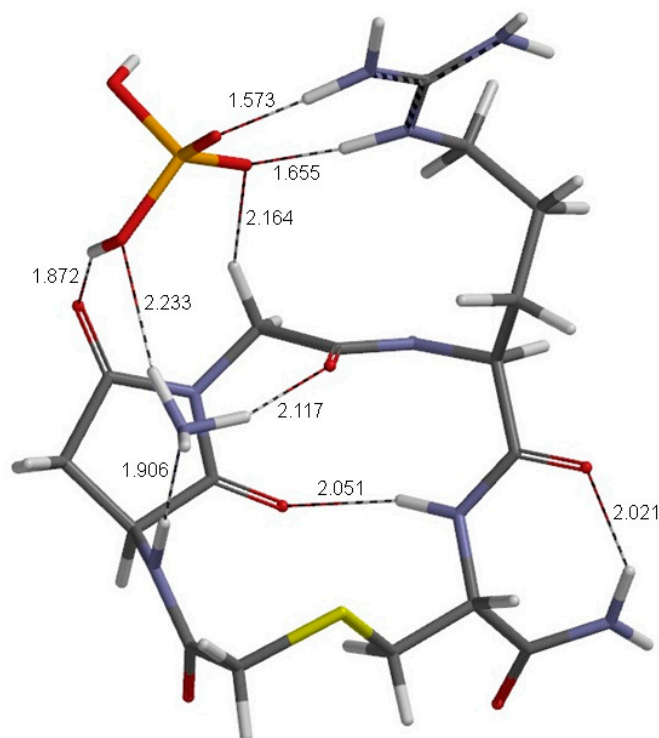
Figure 9. The geometry of PC (product complex) directly connected to TS2 (Figure 8). Selected interatomic distances are shown in Å. Grey: carbon; white: hydrogen; blue: nitrogen; red: oxygen; orange: phosphorus; yellow: sulfur.

3. Computational Methods

All calculations in this work were performed by DFT with the B3LYP functional using Spartan '14 [91]. Geometry optimizations and vibrational frequency calculations were performed in the gas phase using the 6-31G(d) basis set, and the gas-phase electronic energies were recalculated using the 6-31+G(d,p) basis set. Moreover, hydration Gibbs energies were calculated at the gas-phase optimized geometries by the SM8 continuum model [86,87]; the 6-31G(d) basis set was used for these calculations because it produces stable partial atomic charges and is recommended by the developers of the SM8 model [92]. By the vibrational frequency calculations, all the geometries reported in this paper were confirmed to be an energy minimum (with no imaginary frequency) or a transition state (with a single imaginary frequency), and their relative energies were corrected for the ZPE. Moreover, IRC calculations were performed from the located transition states followed by full geometry optimizations in order to confirm the energy minima connected by each transition state.

4. Conclusions

By the B3LYP DFT method, we have computationally revealed a phosphate-catalyzed mechanism for the succinimide formation from an NGR-containing cyclic peptide, c[CH$_2$CO-NGRC]-NH$_2$, which we named CP15. From the reactant complex, in which an $H_2PO_4^-$ ion is bound with CP15 (deprotonated form) by a nine-point interaction involving all of the Asn, Gly, and Arg residues, an intramolecular cyclization occurs with an $H_2PO_4^-$-mediated double proton transfer to form a five-membered ring tetrahedral intermediate having an OH and an NH$_2$ group on the same carbon atom. The calculated activation barrier for this step (90.9 kJ·mol^{-1}) fell within the range of typical

activation energies for nonenzymatic Asn deamidation. The tetrahedral intermediate, once protonated at the NH$_2$ group, was shown to easily undergo NH$_3$ elimination leading to the succinimide formation. Thus, this study has revealed possible catalytic roles of the phosphate buffer and the Arg guanidino group on the succinimide formation from the NGR motif. Further studies on the NGR deamidation are now in progress.

Abbreviations

CP	Cyclic peptide
DFT	Density functional theory
IRC	Intrinsic reaction coordinate
*iso*DGR	*iso*Asp-Gly-Arg
NGR	Asn-Gly-Arg
PC	Product complex
RC	Reactant complex
TH	Tetrahedral intermediate
TS	Transition state
ZPE	Zero-point energy

References

1. Geiger, T.; Clarke, S. Deamidation, isomerization, and racemization at asparaginyl and aspartyl residues in peptides. Succinimide-linked reactions that contribute to protein degradation. *J. Biol. Chem.* **1987**, *262*, 785–794. [PubMed]

2. Capasso, S.; Mazzarella, L.; Sica, F.; Zagari, A. Deamidation via cyclic imide in asparaginyl peptides. *Pept. Res.* **1989**, *2*, 195–200. [PubMed]

3. Stephenson, R.C.; Clarke, S. Succinimide formation from aspartyl and asparaginyl peptides as a model for the spontaneous degradation of proteins. *J. Biol. Chem.* **1989**, *264*, 6164–6170. [PubMed]

4. Patel, K.; Borchardt, R.T. Chemical pathways of peptide degradation. II. Kinetics of deamidation of an asparaginyl residue in a model hexapeptide. *Pharm. Res.* **1990**, *7*, 703–711. [CrossRef] [PubMed]

5. Patel, K.; Borchardt, R.T. Chemical pathways of peptide degradation. III. Effect of primary sequence on the pathways of deamidation of asparaginyl residues in hexapeptides. *Pharm. Res.* **1990**, *7*, 787–793. [CrossRef] [PubMed]

6. Tyler-Cross, R.; Schirch, V. Effects of amino acid sequence, buffers, and ionic strength on the rate and mechanism of deamidation of asparagine residues in small peptides. *J. Biol. Chem.* **1991**, *266*, 22549–22556. [PubMed]

7. Clarke, S.; Stephenson, R.C.; Lowenson, J.D. Lability of asparagine and aspartic acid residues in proteins and peptides: Spontaneous deamidation and isomerization reactions. In *Stability of Protein Pharmaceuticals, Part A: Chemical and Physical Pathways of Protein Degradation*; Ahern, T.J., Manning, M.C., Eds.; Plenum Press: New York, NY, USA, 1992; pp. 1–29.

8. Robinson, N.E.; Robinson, Z.W.; Robinson, B.R.; Robinson, A.L.; Robinson, J.A.; Robinson, M.L.; Robinson, A.B. Structure-dependent nonenzymatic deamidation of glutaminyl and asparaginyl pentapeptides. *J. Pept. Res.* **2004**, *63*, 426–436. [CrossRef] [PubMed]

9. Robinson, N.E.; Robinson, A.B. *Molecular Clocks: Deamidation of Asparaginyl and Glutaminyl Residues in Peptides and Proteins*; Althouse Press: Cave Junction, OR, USA, 2004.

10. Weintraub, S.J.; Deverman, B.E. Chronoregulation by asparagine deamidation. *Sci. STKE* **2007**, *2007*, re7. [CrossRef] [PubMed]

11. Connolly, B.D.; Tran, B.; Moore, J.M.R.; Sharma, V.K.; Kosky, A. Specific catalysis of asparaginyl deamidation by carboxylic acids: Kinetic, thermodynamic, and quantitative structure-property relationship analyses. *Mol. Pharm.* **2014**, *11*, 1345–1358. [CrossRef] [PubMed]

12. Manabe, N.; Kirikoshi, R.; Takahashi, O. Glycolic acid-catalyzed deamidation of asparagine residues in degrading PLGA matrices: A computational study. *Int. J. Mol. Sci.* **2015**, *16*, 7261–7272. [CrossRef] [PubMed]

13. Takahashi, O.; Manabe, N.; Kirikoshi, R. A computational study of the mechanism of succinimide formation in the Asn–His sequence: Intramolecular catalysis by the His side chain. *Molecules* **2016**, *21*, 327. [CrossRef] [PubMed]

14. Takahashi, O. Two-water-assisted racemization of the succinimide intermediate formed in proteins: A computational model study. *Health* **2013**, *5*, 2018–2021. [CrossRef]

15. Takahashi, O.; Kirikoshi, R.; Manabe, N. Racemization of the succinimide intermediate formed in proteins and peptides: A computational study of the mechanism catalyzed by dihydrogen phosphate ion. *Int. J. Mol. Sci.* **2016**, *17*, 1698. [CrossRef] [PubMed]

16. Arap, W.; Pasqualini, R.; Ruoslahti, E. Cancer treatment by targeted drug delivery to tumor vasculature in a mouse model. *Science* **1998**, *279*, 377–380. [CrossRef] [PubMed]

17. Ellerby, H.M.; Arap, W.; Ellerby, L.M.; Kain, R.; Andrusiak, R.; Rio, G.D.; Krajewski, S.; Lombardo, C.R.; Rao, R.; Ruoslahti, E.; et al. Anti-cancer activity of targeted pro-apoptotic peptides. *Nat. Med.* **1999**, *5*, 1032–1038. [PubMed]

18. Pasqualini, R.; Koivunen, E.; Kain, R.; Lahdenranta, J.; Sakamoto, M.; Stryhn, A.; Ashmun, R.A.; Shapiro, L.H.; Arap, W.; Ruoslahti, E. Aminopeptidase N is a receptor for tumor-homing peptides and a target for inhibiting angiogenesis. *Cancer Res.* **2000**, *60*, 722–727. [PubMed]

19. Liu, L.; Liu, L.; Anderson, W.F.; Beart, R.W.; Gordon, E.M.; Hall, F.L. Incorporation of tumor vasculature targeting motifs into Moloney murine leukemia virus Env escort proteins enhances retrovirus binding and transduction of human endothelial cells. *J. Virol.* **2000**, *74*, 5320–5328. [CrossRef] [PubMed]

20. Curnis, F.; Sacchi, A.; Borgna, L.; Magni, F.; Gasparri, A.; Corti, A. Enhancement of tumor necrosis factor α antitumor immunotherapeutic properties by targeted delivery to aminopeptidase N (CD13). *Nat. Biotechnol.* **2000**, *18*, 1185–1190. [PubMed]

21. Grifman, M.; Trepel, M.; Speece, P.; Gilbert, L.B.; Arap, W.; Pasqualini, R.; Weitzman, M.D. Incorporation of tumor-targeting peptides into recombinant adeno-associated virus capsids. *Mol. Ther.* **2001**, *3*, 964–975. [CrossRef] [PubMed]

22. Curnis, F.; Arrigoni, G.; Sacchi, A.; Fischetti, L.; Arap, W.; Pasqualini, R.; Corti, A. Differential binding of drugs containing the NGR motif to CD13 isoforms in tumor vessels, epithelia, and myeloid cells. *Cancer Res.* **2002**, *62*, 867–874. [PubMed]

23. Curnis, F.; Sacchi, A.; Corti, A. Improving chemotherapeutic drug penetration in tumors by vasculature targeting and barrier alteration. *J. Clin. Investig.* **2002**, *110*, 475–482. [CrossRef] [PubMed]

24. Colombo, G.; Curnis, F.; de Mori, G.M.S.; Gasparri, A.; Longoni, C.; Sacchi, A.; Longhi, R.; Corti, A. Structure-activity relationship of linear and cyclic peptides containing the NGR tumor-homing motif. *J. Biol. Chem.* **2002**, *277*, 47891–47897. [CrossRef] [PubMed]

25. Pastorino, F.; Brignole, C.; Marimpietri, D.; Cilli, M.; Gambini, C.; Ribatti, D.; Longhi, R.; Allen, T.M.; Corti, A.; Ponzoni, M. Vascular damage and anti-angiogenic effects of tumor vessel-targeted liposomal chemotherapy. *Cancer Res.* **2003**, *63*, 7400–7409. [PubMed]

26. Zarovni, N.; Monaco, L.; Corti, A. Inhibition of tumor growth by intramuscular injection of cDNA encoding tumor necrosis factor α coupled to NGR and RGD tumor-homing peptides. *Hum. Gene Ther.* **2004**, *15*, 373–382. [CrossRef] [PubMed]

27. Sacchi, A.; Gasparri, A.; Curnis, F.; Bellone, M.; Corti, A. Crucial role for interferon γ in the synergism between tumor vasculature-targeted tumor necrosis factor α (NGR-TNF) and doxorubicin. *Cancer Res.* **2004**, *64*, 7150–7155. [CrossRef] [PubMed]

28. Corti, A.; Ponzoni, M. Tumor vascular targeting with tumor necrosis factor α and chemotherapeutic drugs. *Ann. N. Y. Acad. Sci.* **2004**, *1028*, 104–112. [CrossRef] [PubMed]

29. Dirksen, A.; Langereis, S.; de Waal, B.F.M.; van Genderen, M.H.P.; Meijer, E.W.; de Lussanet, Q.G.; Hackeng, T.M. Design and synthesis of a bimodal target-specific contrast agent for angiogenesis. *Org. Lett.* **2004**, *6*, 4857–4860. [CrossRef] [PubMed]

30. Curnis, F.; Gasparri, A.; Sacchi, A.; Cattaneo, A.; Magni, F.; Corti, A. Targeted delivery of IFNγ to tumor vessels uncouples antitumor from counterregulatory mechanisms. *Cancer Res.* **2005**, *65*, 2906–2913. [CrossRef] [PubMed]

31. Yokoyama, Y.; Ramakrishnan, S. Addition of an aminopeptidase N-binding sequence to human endostatin improves inhibition of ovarian carcinoma growth. *Cancer* **2005**, *104*, 321–331. [CrossRef] [PubMed]

32. Sacchi, A.; Gasparri, A.; Gallo-Stampino, C.; Toma, S.; Curnis, F.; Corti, A. Synergistic antitumor activity of cisplatin, paclitaxel, and gemcitabine with tumor vasculature-targeted tumor necrosis factor-α. *Clin. Cancer Res.* **2006**, *12*, 175–182. [CrossRef] [PubMed]

33. Di Matteo, P.; Curnis, F.; Longhi, R.; Colombo, G.; Sacchi, A.; Crippa, L.; Protti, M.P.; Ponzoni, M.; Toma, S.; Corti, A. Immunogenic and structural properties of the Asn-Gly-Arg (NGR) tumor neovasculature-homing motif. *Mol. Immunol.* **2006**, *43*, 1509–1518. [CrossRef] [PubMed]

34. Majhen, D.; Gabrilovac, J.; Eloit, M.; Richardson, J.; Ambriović-Ristov, A. Disulfide bond formation in NGR fiber-modified adenovirus is essential for retargeting to aminopeptidase N. *Biochem. Biophys. Res. Commun.* **2006**, *348*, 278–287. [CrossRef] [PubMed]

35. Pastorino, F.; Brignole, C.; di Paolo, D.; Nico, B.; Pezzolo, A.; Marimpietri, D.; Pagnan, G.; Piccardi, F.; Cilli, M.; Longhi, R.; et al. Targeting liposomal chemotherapy via both tumor cell-specific and tumor vasculature-specific ligands potentiates therapeutic efficacy. *Cancer Res.* **2006**, *66*, 10073–10082. [CrossRef] [PubMed]

36. Crippa, L.; Gasparri, A.; Sacchi, A.; Ferrero, E.; Curnis, F.; Corti, A. Synergistic damage of tumor vessels with ultra low-dose endothelial-monocyte activating polypeptide-II and neovasculature-targeted tumor necrosis factor-α. *Cancer Res.* **2008**, *68*, 1154–1161. [CrossRef] [PubMed]

37. Kessler, T.; Schwöppe, C.; Liersch, R.; Schliemann, C.; Hintelmann, H.; Bieker, R.; Berdel, W.E.; Mesters, R.M. Generation of fusion proteins for selective occlusion of tumor vessels. *Curr. Drug. Discov. Technol.* **2008**, *5*, 1–8. [PubMed]

38. Corti, A.; Curnis, F.; Arap, W.; Pasqualini, R. The neovasculature homing motif NGR: More than meets the eye. *Blood* **2008**, *112*, 2628–2635. [CrossRef] [PubMed]

39. Oostendorp, M.; Douma, K.; Hackeng, T.M.; Dirksen, A.; Post, M.J.; van Zandvoort, M.A.M.J.; Backes, W.H. Quantitative molecular magnetic resonance imaging of tumor angiogenesis using cNGR-labeled paramagnetic quantum dots. *Cancer Res.* **2008**, *68*, 7676–7683. [CrossRef] [PubMed]

40. Gasparri, A.M.; Jachetti, E.; Colombo, B.; Sacchi, A.; Curnis, F.; Rizzardi, G.-P.; Traversari, C.; Bellone, M.; Corti, A. Critical role of indoleamine 2,3-dioxygenase in tumor resistance to repeated treatments with targeted IFNγ. *Mol. Cancer Ther.* **2008**, *7*, 3859–3866. [CrossRef] [PubMed]

41. Bieker, R.; Kessler, T.; Schwöppe, C.; Padró, T.; Persigehl, T.; Bremer, C.; Dreischalück, J.; Kolkmeyer, A.; Heindel, W.; Mesters, R.M.; et al. Infarction of tumor vessels by NGR-peptide-directed targeting of tissue factor: Experimental results and first-in-man experience. *Blood* **2009**, *113*, 5019–5027. [CrossRef] [PubMed]

42. Jullienne, B.; Vigant, F.; Muth, E.; Chaligné, R.; Bouquet, C.; Giraudier, S.; Perricaudet, M.; Benihoud, K. Efficient delivery of angiostatin K1–5 into tumors following insertion of an NGR peptide into adenovirus capsid. *Gene Ther.* **2009**, *16*, 1405–1415. [CrossRef] [PubMed]

43. Wang, X.; Wang, Y.; Chen, X.; Wang, J.; Zhang, X.; Zhang, Q. NGR-modified micelles enhance their interaction with CD13-overexpressing tumor and endothelial cells. *J. Control. Release* **2009**, *139*, 56–62. [CrossRef] [PubMed]

44. Gregorc, V.; Citterio, G.; Vitali, G.; Spreafico, A.; Scifo, P.; Borri, A.; Donadoni, G.; Rossoni, G.; Corti, A.; Caligaris-Cappio, F.; et al. Defining the optimal biological dose of NGR-hTNF, a selective vascular targeting agent, in advanced solid tumors. *Eur. J. Cancer* **2010**, *46*, 198–206. [CrossRef] [PubMed]

45. Murase, Y.; Asai, T.; Katanasaka, Y.; Sugiyama, T.; Shimizu, K.; Maeda, N.; Oku, N. A novel DDS strategy, "dual-targeting", and its application for antineovascular therapy. *Cancer Lett.* **2010**, *287*, 165–171. [CrossRef] [PubMed]

46. Mari, S.; Invernizzi, C.; Spitaleri, A.; Alberici, L.; Ghitti, M.; Bordignon, C.; Traversari, C.; Rizzardi, G.-P.; Musco, G. 2D TR-NOESY experiments interrogate and rank ligand–receptor interactions in living human cancer cells. *Angew. Chem. Int. Ed.* **2010**, *49*, 1071–1074. [CrossRef] [PubMed]

47. Van Laarhoven, H.W.M.; Fiedler, W.; Desar, I.M.E.; van Asten, J.J.A.; Marréaud, S.; Lacombe, D.; Govaerts, A.-S.; Bogaerts, J.; Lasch, P.; Timmer-Bonte, J.N.H.; et al. Phase I clinical and magnetic resonance imaging study of the vascular agent NGR-hTNF in patients with advanced cancers (European organization for research and treatment of cancer study 16041). *Clin. Cancer Res.* **2010**, *16*, 1315–1323. [CrossRef] [PubMed]

48. Curnis, F.; Cattaneo, A.; Longhi, R.; Sacchi, A.; Gasparri, A.M.; Pastorino, F.; di Matteo, P.; Traversari, C.; Bachi, A.; Ponzoni, M.; et al. Critical role of flanking residues in NGR-to-*iso*DGR transition and CD13/integrin receptor switching. *J. Biol. Chem.* **2010**, *285*, 9114–9123. [CrossRef] [PubMed]

49. Gregorc, V.; Zucali, P.A.; Santoro, A.; Ceresoli, G.L.; Citterio, G.; de Pas, T.M.; Zilembo, N.; de Vincenzo, F.; Simonelli, M.; Rossoni, G.; et al. Phase II study of asparagine-glycine-arginine–human tumor necrosis factor α, a selective vascular targeting agent, in previously treated patients with malignant pleural mesothelioma. *J. Clin. Oncol.* **2010**, *28*, 2604–2611. [CrossRef] [PubMed]

50. Loi, M.; Marchiò, S.; Becherini, P.; di Paolo, D.; Soster, M.; Curnis, F.; Brignole, C.; Pagnan, G.; Perri, P.; Caffa, I.; et al. Combined targeting of perivascular and endothelial tumor cells enhances anti-tumor efficacy of liposomal chemotherapy in neuroblastoma. *J. Control. Release* **2010**, *145*, 66–73. [CrossRef] [PubMed]

51. Son, S.; Singha, K.; Kim, W.J. Bioreducible BPEI-SS-PEG-cNGR polymer as a tumor targeted nonviral gene carrier. *Biomaterials* **2010**, *31*, 6344–6354. [CrossRef] [PubMed]

52. Santoro, A.; Rimassa, L.; Sobrero, A.F.; Citterio, G.; Sclafani, F.; Carnaghi, C.; Pessino, A.; Caprioni, F.; Andretta, V.; Tronconi, M.C.; et al. Phase II study of NGR-hTNF, a selective vascular targeting agent, in patients with metastatic colorectal cancer after failure of standard therapy. *Eur. J. Cancer* **2010**, *46*, 2746–2752. [CrossRef] [PubMed]

53. Wickström, M.; Larsson, R.; Nygren, P.; Gullbo, J. Aminopeptidase N (CD13) as a target for cancer chemotherapy. *Cancer Sci.* **2011**, *102*, 501–508. [CrossRef] [PubMed]

54. Gregorc, V.; de Braud, F.G.; de Pas, T.M.; Scalamogna, R.; Citterio, G.; Milani, A.; Boselli, S.; Catania, C.; Donadoni, G.; Rossoni, G.; et al. Phase I study of NGR-hTNF, a selective vascular targeting agent, in combination with cisplatin in refractory solid tumors. *Clin. Cancer Res.* **2011**, *17*, 1964–1972. [CrossRef] [PubMed]

55. Zhang, B.; Gao, B.; Dong, S.; Zhang, Y.; Wu, Y. Anti-tumor efficacy and pre-clinical immunogenicity of IFNα2a-NGR. *Regul. Toxicol. Pharmacol.* **2011**, *60*, 73–78. [CrossRef] [PubMed]

56. Corti, A.; Curnis, F. Tumor vasculature targeting through NGR peptide-based drug delivery systems. *Curr. Pharm. Biotechnol.* **2011**, *12*, 1128–1134. [CrossRef] [PubMed]

57. Dunne, M.; Zheng, J.; Rosenblat, J.; Jaffray, D.A.; Allen, C. APN/CD13-targeting as a strategy to alter the tumor accumulation of liposomes. *J. Control. Release* **2011**, *154*, 298–305. [CrossRef] [PubMed]

58. Zauderer, M.G.; Krug, L.M. Novel therapies in phase II and III trials for malignant pleural mesothelioma. *J. Natl. Compr. Cancer Netw.* **2012**, *10*, 42–47.

59. Zou, M.; Zhang, L.; Xie, Y.; Xu, W. NGR-based strategies for targeting delivery of chemotherapeutics to tumor vasculature. *Anti Cancer Agents Med. Chem.* **2012**, *12*, 239–246. [CrossRef]

60. Kapoor, P.; Singh, H.; Gautam, A.; Chaudhary, K.; Kumar, R.; Raghava, G.P.S. TumorHoPe: A database of tumor homing peptides. *PLoS ONE* **2012**, *7*, e35187. [CrossRef] [PubMed]

61. Lorusso, D.; Scambia, G.; Amadio, G.; di Legge, A.; Pietragalla, A.; de Vincenzo, R.; Masciullo, V.; di Stefano, M.; Mangili, G.; Citterio, G.; et al. Phase II study of NGR-hTNF in combination with doxorubicin in relapsed ovarian cancer patients. *Br. J. Cancer* **2012**, *107*, 37–42. [CrossRef] [PubMed]

62. Corti, A.; Pastorino, F.; Curnis, F.; Arap, W.; Ponzoni, M.; Pasqualini, R. Targeted drug delivery and penetration into solid tumors. *Med. Res. Rev.* **2012**, *32*, 1078–1091. [CrossRef] [PubMed]

63. Li, Z.J.; Cho, C.H. Peptides as targeting probes against tumor vasculature for diagnosis and drug delivery. *J. Transl. Med.* **2012**, *10*, S1. [CrossRef] [PubMed]

64. Soudy, R.; Ahmed, S.; Kaur, K. NGR peptide ligands for targeting CD13/APN identified through peptide array screening resemble fibronectin sequences. *ACS Comb. Sci.* **2012**, *14*, 590–599. [CrossRef] [PubMed]

65. Zucali, P.A.; Simonelli, M.; de Vincenzo, F.; Lorenzi, E.; Perrino, M.; Bertossi, M.; Finotto, R.; Naimo, S.; Balzarini, L.; Bonifacio, C.; et al. Phase I and pharmacodynamic study of high-dose NGR–hTNF in patients with refractory solid tumours. *Br. J. Cancer* **2013**, *108*, 58–63. [CrossRef] [PubMed]

66. Corti, A.; Curnis, F.; Rossoni, G.; Marcucci, F.; Gregorc, V. Peptide-mediated targeting of cytokines to tumor vasculature: The NGR-hTNF example. *BioDrugs* **2013**, *27*, 591–603. [CrossRef] [PubMed]

67. Di Paolo, D.; Pastorino, F.; Zuccari, G.; Caffa, I.; Loi, M.; Marimpietri, D.; Brignole, C.; Perri, P.; Cilli, M.; Nico, B.; et al. Enhanced anti-tumor and anti-angiogenic efficacy of a novel liposomal fenretinide on human neuroblastoma. *J. Control. Release* **2013**, *170*, 445–451. [CrossRef] [PubMed]

68. D'Onofrio, N.; Caraglia, M.; Grimaldi, A.; Marfella, R.; Servillo, L.; Paolisso, G.; Balestrieri, M.L. Vascular-homing peptides for targeted drug delivery and molecular imaging: Meeting the clinical challenges. *Biochim. Biophys. Acta* **2014**, *1846*, 1–12. [CrossRef] [PubMed]

69. Parmiani, G.; Pilla, L.; Corti, A.; Doglioni, C.; Cimminiello, C.; Bellone, M.; Parolini, D.; Russo, V.; Capocefalo, F.; Maccalli, C. A pilot Phase I study combining peptide-based vaccination and NGR-hTNF vessel targeting therapy in metastatic melanoma. *OncoImmunology* **2014**, *3*, e963406. [CrossRef] [PubMed]

70. Liu, C.; Yang, Y.; Chen, L.; Lin, Y.-L.; Li, F. A unified mechanism for aminopeptidase N-based tumor cell motility and tumor-homing therapy. *J. Biol. Chem.* **2014**, *289*, 34520–34529. [CrossRef] [PubMed]

71. Enyedi, K.N.; Czajlik, A.; Knapp, K.; Láng, A.; Majer, Z.; Lajkó, E.; Kőhidai, L.; Perczel, A.; Mező, G. Development of cyclic NGR peptides with thioether linkage: Structure and dynamics determining deamidation and bioactivity. *J. Med. Chem.* **2015**, *58*, 1806–1817. [CrossRef] [PubMed]

72. Zuccari, G.; Milelli, A.; Pastorino, F.; Loi, M.; Petretto, A.; Parise, A.; Marchetti, C.; Minarini, A.; Cilli, M.; Emionite, L.; et al. Tumor vascular targeted liposomal-bortezomib minimizes side effects and increases therapeutic activity in human neuroblastoma. *J. Control. Release* **2015**, *211*, 44–52. [CrossRef] [PubMed]

73. Petrozziello, E.; Sturmheit, T.; Mondino, A. Exploiting cytokines in adoptive T-cell therapy of cancer. *Immunotherapy* **2015**, *7*, 573–584. [CrossRef] [PubMed]

74. Huang, Y.; Cheng, Q.; Jin, X.; Ji, J.-L.; Guo, S.; Zheng, S.; Wang, X.; Cao, H.; Gao, S.; Liang, X.-J.; Du, Q.; Liang, Z. Systemic and tumor-targeted delivery of siRNA by cyclic NGR and *iso*DGR motif-containing peptides. *Biomater. Sci.* **2016**, *4*, 494–510. [CrossRef] [PubMed]

75. Curnis, F.; Fiocchi, M.; Sacchi, A.; Gori, A.; Gasparri, A.; Corti, A. NGR-tagged nano-gold: A new CD13-selective carrier for cytokine delivery to tumors. *Nano Res.* **2016**, *9*, 1393–1408. [CrossRef] [PubMed]

76. Curnis, F.; Longhi, R.; Crippa, L.; Cattaneo, A.; Dondossola, E.; Bachi, A.; Corti, A. Spontaneous formation of L-isoaspartate and gain of function in fibronectin. *J. Biol. Chem.* **2006**, *281*, 36466–36476. [CrossRef] [PubMed]

77. Spitaleri, A.; Mari, S.; Curnis, F.; Traversari, C.; Longhi, R.; Bordignon, C.; Corti, A.; Rizzardi, G.-P.; Musco, G. Structural basis for the interaction of *iso*DGR with the RGD-binding site of αvβ3 integrin. *J. Biol. Chem.* **2008**, *283*, 19757–19768. [CrossRef] [PubMed]

78. Curnis, F.; Sacchi, A.; Gasparri, A.; Longhi, R.; Bachi, A.; Doglioni, C.; Bordignon, C.; Traversari, C.; Rizzardi, G.-P.; Corti, A. Isoaspartate-glycine-arginine: A new tumor vasculature-targeting motif. *Cancer Res.* **2008**, *68*, 7073–7082. [CrossRef] [PubMed]

79. Pathuri, G.; Sahoo, K.; Awasthi, V.; Gali, H. Synthesis and in vivo evaluation of Tc-99m-labeled cyclic C*iso*DGRC peptide conjugates for targeting αvβ3 integrin expression. *Bioorg. Med. Chem. Lett.* **2010**, *20*, 5969–5972. [CrossRef] [PubMed]

80. Frank, A.O.; Otto, E.; Mas-Moruno, C.; Schiller, H.B.; Marinelli, L.; Cosconati, S.; Bochen, A.; Vossmeyer, D.; Zahn, G.; Stragies, R.; et al. Conformational control of integrin-subtype selectivity in *iso*DGR peptide motifs: A biological switch. *Angew. Chem. Int. Ed.* **2010**, *49*, 9278–9281. [CrossRef] [PubMed]

81. Spitaleri, A.; Ghitti, M.; Mari, S.; Alberici, L.; Traversari, C.; Rizzardi, G.-P.; Musco, G. Use of metadynamics in the design of isoDGR-based αvβ3 antagonists to fine-tune the conformational ensemble. *Angew. Chem. Int. Ed.* **2011**, *50*, 1832–1836. [CrossRef] [PubMed]

82. Corti, A.; Curnis, F. Isoaspartate-dependent molecular switches for integrin–ligand recognition. *J. Cell Sci.* **2011**, *124*, 515–522. [CrossRef] [PubMed]

83. Ghitti, M.; Spitaleri, A.; Valentinis, B.; Mari, S.; Asperti, C.; Traversari, C.; Rizzardi, G.P.; Musco, G. Molecular dynamics reveal that isoDGR-containing cyclopeptides are true αvβ3 antagonists unable to promote integrin allostery and activation. *Angew. Chem. Int. Ed.* **2012**, *51*, 7702–7705. [CrossRef] [PubMed]

84. Mingozzi, M.; Dal Corso, A.; Marchini, M.; Guzzetti, I.; Civera, M.; Piarulli, U.; Arosio, D.; Belvisi, L.; Potenza, D.; Pignataro, L.; et al. Cyclic *iso*DGR peptidomimetics as low-nanomolar αvβ3 integrin ligands. *Chem. Eur. J.* **2013**, *19*, 3563–3567. [CrossRef] [PubMed]

85. Curnis, F.; Sacchi, A.; Longhi, R.; Colombo, B.; Gasparri, A.; Corti, A. IsoDGR-tagged albumin: A new αvβ3 selective carrier for nanodrug delivery to tumors. *Small* **2013**, *9*, 673–678. [CrossRef] [PubMed]

86. Marenich, A.V.; Olson, R.M.; Kelly, C.P.; Cramer, C.J.; Truhlar, D.G. Self-consistent reaction field model for aqueous and nonaqueous solutions based on accurate polarized partial charges. *J. Chem. Theory Comput.* **2007**, *3*, 2011–2033. [CrossRef] [PubMed]

87. Cramer, C.J.; Truhlar, D.G. A universal approach to solvation modeling. *Acc. Chem. Res.* **2008**, *41*, 760–768. [CrossRef] [PubMed]

88. Takahashi, O.; Oda, A. Amide–iminol tautomerization of the C-terminal peptide groups of aspartic acid residues. Two-water-assisted mechanism, cyclization from the iminol tautomer leading to the tetrahedral intermediate of succinimide formation, and implication to peptide group hydrogen exchange. In *Tyrosine and Aspartic Acid: Properties, Sources and Health Benefits*; Jones, J.E., Morano, D.M., Eds.; Nova Science Publishers: New York, NY, USA, 2012; pp. 131–147.

89. Camaioni, D.M.; Schwerdtfeger, C.A. Comment on "Accurate experimental values for the free energies of hydration of H$^+$, OH$^-$, and H$_3$O$^+$". *J. Phys. Chem. A* **2005**, *109*, 10795–10797. [CrossRef] [PubMed]

90. Aue, D.H.; Webb, H.M.; Bowers, M.T. A thermodynamic analysis of solvation effects on the basicities of alkylamines. An electrostatic analysis of substituent effects. *J. Am. Chem. Soc.* **1976**, *98*, 318–329. [CrossRef]

91. *Spartan '14*, version 1.1.4; Wavefunction, Inc.: Irvine, CA, USA, 2014.

92. Chamberlin, A.C.; Cramer, C.J.; Truhlar, D.G. Performance of SM8 on a test to predict small-molecule solvation free energies. *J. Phys. Chem. B* **2008**, *112*, 8651–8655. [CrossRef] [PubMed]